
Article:
Feng, X., Calcines, A., Sharples, R. M. et al. (8 more authors) (2021) Development of an 11-channel multi wavelength imaging diagnostic for divertor plasmas in MAST Upgrade. Review of Scientific Instruments. 063510. ISSN 0034-6748

https://doi.org/10.1063/5.0043533

Development of an 11-channel Multi Wavelength Imaging diagnostic for divertor plasmas in MAST Upgrade[a)]

X. Feng,[1, a)] A. Calcines, [1] R. M. Sharples, [1] B. Lipschultz, [2] A. Perek, [3] W. A. J. Vijvers, [3,b)] J. R. Harrison, [4] J. S. Allcock,[4] Y. Andrebe, [5] B. P. Duval, [5] R. T. Mumgaard[6,c)], the MAST-U Team and the EUROfusion MST1 Team[d)]

[1]*Centre for Advanced Instrumentation, Durham University, South Road, Durham, DH1 3LE, United Kingdom*
[2]*York Plasma Institute, University of York, York, YO10 5DQ, United Kingdom*
[3]*Dutch Institute for Fundamental Energy Research (DIFFER), De Zaale 20, 5612 AJ Eindhoven, The Netherlands*
[4]*CCFE, Culham Science Centre, Abingdon, Oxon, OX14 3DB, United Kingdom*
[5]*Ecole Polytechnique Fédérale de Lausanne (EPFL), Swiss Plasma Center (SPC), 1015 Lausanne, Switzerland*
[6]*Plasma Science and Fusion Center MIT, Cambridge, Massachusetts 02139, USA*
[b]*Current address: Chromodynamics BV, 5656 AE Eindhoven, The Netherlandsd*
[c]*Current address: Commonwealth Fusion Systems, Cambridge, MA, USA*

(Presented XXXXX; received XXXXX; accepted XXXXX; published online XXXXX)

Divertor detachment and alternative divertor magnetic geometries are predicted to be promising approaches to handle the power exhaust of future fusion devices. In order to understand the detachment process caused by volumetric losses in alternative divertor magnetic geometries, a Multi-Wavelength Imaging (MWI) diagnostic has recently been designed and built for the Mega Amp Spherical Tokamak Upgrade (MAST-U). The MWI diagnostic will simultaneously capture 11 spectrally filtered images of the visible light emitted from divertor plasmas and provide crucial knowledge for the interpretation of observations and modeling efforts. This manuscript presents the optical design, mechanical design, hardware and test results of an 11-channel MWI system with a field of view of 40°. The optical design shows better than 5mm FWHM spatial resolution at the plasma on all 11 channels across the whole field of view. The spread of angle of incidence on the surface of each filter is also analyzed to inform the bandwidth specification of the interference filters. The results of the initial laboratory tests demonstrate that a spatial resolution of better than 5mm FWHM is achieved for all 11 channels, meeting the specifications required for accurate tomography.

I. INTRODUCTION

Heat exhaust physics in the divertor is one of the main challenges in realizing magnetic confinement fusion. Divertor detachment, which involves a variety of atomic and molecular processes and can lead to reduced heat and particle fluxes on the divertor, is predicted to be crucial for handling the heat exhaust issue[1,2], and it is well known that alternative divertor magnetic topology could further facilitate the reduced heat load[3,4]. MAST Upgrade (MAST-U) will have unprecedented flexibility to tailor the magnetic geometry to improve the understanding of detachment onset and control in conventional and alternative divertor configurations[5]. In order to understand the dynamics of the detachment process and the physics of detachment in the MAST-U divertor, a Multi-Wavelength Imaging (MWI) diagnostic has recently been built to diagnose the emission front and infer recombination rates from Balmer line intensities[6,7]. The MWI will also measure 2D distributions of electron density and electron temperature in divertor plasmas through line intensity ratios of Deuterium Balmer lines[8] and helium singlet and triplet lines[9-11]. The inferred 2D map of plasma parameters, combined with localized measurements from Langmuir probes/Thomson scattering systems and 1D emission-weighted plasma profiles from spectroscopy, will provide crucial knowledge for the interpretation of observations. MWI data will also be used as input to integrated data analysis[12] and for constraining divertor plasma simulations. The MWI is a diagnostic which uses a polychromatic configuration with narrow bandwidth interference filters and CMOS cameras to simultaneously capture 11 spectrally filtered images (380nm-750nm) of divertor plasmas. The design has been developed based on a previous 4-channel Multi-Spectral Imaging system (MSI)[13] and a 10-channel Multispectral Advanced Narrowband Tokamak Imaging System (MANTIS)[14,15] on the TCV tokamak. The design of the MWI was extended to 11 channels to allow the future incorporation of a coherence imaging channel for measurements of plasma flows[16] and Stark broadening[17]. Comparing with previous multiple spectral imaging diagnostics which use beam splitter or dichroic mirror approaches, the polychromatic layout is better able to support large numbers filtered image views and emission lines closely spaced in wavelength. This paper focuses on the systematic analysis of optical design, mechanical design with integration of in-situ calibration method and quantification of the image quality of the multi-

[a)]Author to whom correspondence should be addressed: xiande.feng@durham.ac.uk.
[d)] See the EUROfusion MST1 Team list of B. Labit et al. Nucl. Fusion 59 086020, 2019

wavelength imaging instrument, which are not discussed before in the similar systems.

II. OPTICAL PERFORMANCE OF THE MWI SYSTEM

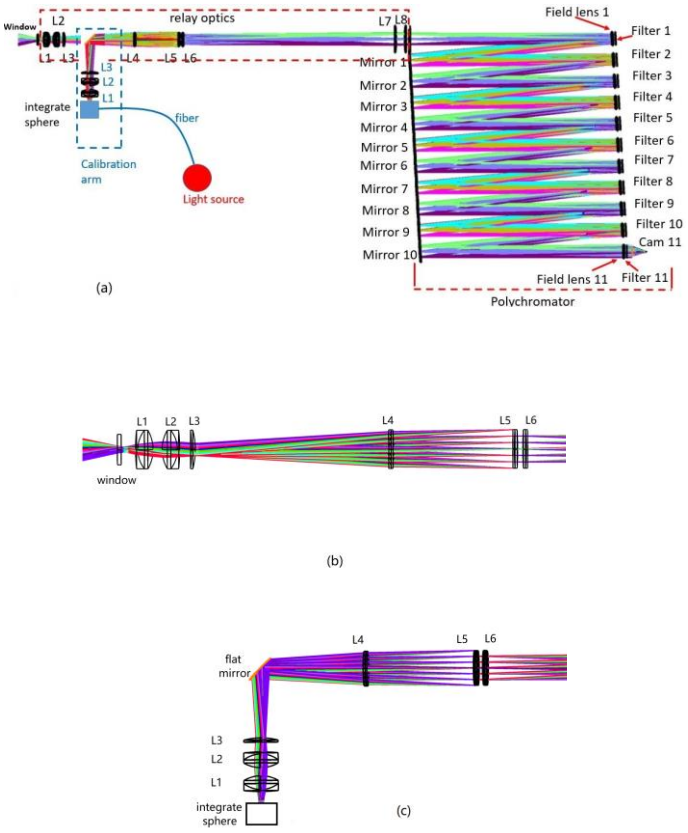

FIG. 1. (a) Zemax ray tracing of MWI optical design including the schematic drawing of calibration arm. Only one camera is shown (on channel 11). (b) Zoom-in view of L1-L6 in the original relay optics. (c)Zoom-in view of the optics (L1-L3 and flat mirror) in calibration arm.

In order to view the whole divertor on MAST-U, the MWI optics have a field of view of 40° and are composed of separate relay optics and polychromatic optics. Figure 1(a) shows a Zemax ray tracing of the MWI optical design including the schematic drawing of calibration arm. The relay optics are composed of six 50mm aperture off-the-shelf commercial lenses (L1-L6 in figure 1) and two 100mm aperture Plano Convex lenses (L7-L8 in figure 1) with anti-reflection coating to reduce the intensity loss. In which, L1 and L2 are Achromatic Doublet lenses with a focus length of 75mm (Thorlabs AC508-075-A), L3 is a Positive Meniscus Lens with 300mm focal length (Thorlabs LE1985-A), L4 is an Achromatic Doublet lenses with a focus length of 500mm (Thorlabs AC508-500-A), L5 and L6 are Achromatic Doublet lenses with a focus length of 750mm (Thorlabs AC508-750-A), and L7-L8 have a focal length of 800mm (OptoSigma SLB100-800PM). Figure 1(b) shows the zoom-in view of L1-L6 in the relay optics and figure 1(c) shows the zoom-in view of the optics- L1-L3 which have the same arrangement as the L1-L3 in the original arm and a mirror which will be manually inserted into a 60mm cage to switch to the in-situ calibration. The relay optics generate an intermediate image of the object field at a position ~20mm after the last lens in the relay optics (L8). This intermediate image can be used for in-situ focus adjustment and image quality assessment for all the cameras. The polychromator, which has the same configuration as MANTIS[14,15], is in turn based on the original polychromator design for the Motional-Stark Effect diagnostic on Alcator C-MOD[18]. Each polychromator in the MWI is composed of a field lens with focal length of 750mm (achromatic doublet lens), a bandpass interference filter, a dielectric coating concave mirror with a curvature radius of 768mm, camera lens and a CMOS camera. The polychromator is operating off-axis with a cavity angle of θ=3° following a trade-off study between image quality and space required for the field lens, filter holder and camera. The focal length of the field lens is chosen to be the same as the distance from the intermediate image position to the field lens so the beam after the field lens becomes collimated. The filter located after the field lens transmits the wavelength of interest and reflect the rest of the spectral range to the field lens again to produce an intermediate image on a concave mirror with a focal length of half that of the field lens. The field mirror acts as a 1:1 pupil reimaging system for the next channel. This process is repeated over the cavity until the last channel is reached.

For the optical performance of the MWI optics, it is desired that the image quality over the whole field view should be less than 5mm FWHM to enable high quality tomographic analysis. However, as the MWI has a very large field of view, this is challenging for the optical design. The optical performance has therefore been analyzed extensively in Zemax. Figure 2 shows the focus position (the distance from camera lens to sensor) and image quality (spatial resolution at the plasma) as a function of channel number. The cameras lens used in the Zemax analysis is a paraxial lens instead of the real camera lens for which the Zemax prescription was not available. The focus position is a function of wavelength and channel, as shown in the top panel in figure 2, which shows that the position of the focus increases with channel numbers for the same wavelength and that within the same channel, the focus position varies with wavelength. This means that focus adjustment is required when changing the filter and an in-situ focus calibration method is needed (see below). The bottom panel in figure 2 shows that the image quality deteriorates with channel number as expected due to the effect of additional optics for both wavelengths, and the image quality after the third channel does not meet our requirement. For this analysis, the paraxial lens in front of the detector has the same aperture stop setting for all the channels and is equal to the maximum lens aperture. The image quality plotted here is an average of eleven points in the field of view with one point on axis and two orthogonal points on the 5°, 10°, 20°, 30° & 40° field of view circle. Further analysis shows which aberrations (e.g. spherical aberration) in the system are accumulating with channel number leading to the deterioration of image quality. The polychromator has the capability to self-cancel certain off-axis aberrations like

coma which depend on the angle of field of view due to the flip of the image by the concave mirror on consecutive channels, as described in detail in reference[18]. However, the spherical aberration, which dominates other aberrations due to the wide field of view of the system, is accumulated and the best way to minimize such aberrations is to reduce the numerical aperture by stopping down the camera lens.

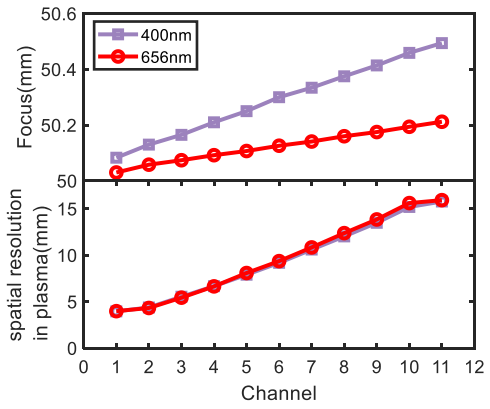

FIG. 2. Focus position of camera lens and image quality with MWI channel numbers.

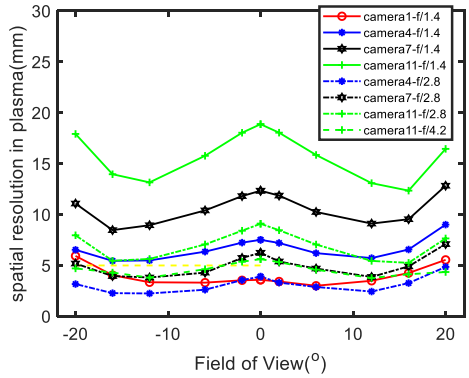

FIG. 3. Spatial resolution at the plasma with field of view on different channel numbers and at different focal ratios.

Figure 3 shows the spatial resolution of the MWI system as a function of channel number and field of view from the Zemax model. The solid lines show the results at the maximum paraxial lens aperture of f/1.4. It can be seen that the spatial resolution from Channel 4 onwards at full aperture will be larger than our requirement, but that stopping down the lens to f/2.8 could improve the image quality to make it less than 5mm FWHM over the whole field of view. From Channel 7 onwards, further stopping down of the paraxial lens to f/4.2 is needed to maintain the image quality. Although stopping down the camera lens will lead to reduced throughput to the sensor, this strategy can work for the MWI system since the brightness of different lines (wavelengths) varies significantly in divertor plasmas. For example, the Dα line can be 1000 times brighter than Dε in a typical divertor plasma and so the Dα filter could be put into one of the latter channels to achieve good spatial resolution with still enough signal on the camera sensor. This strategy has been verified with the MANTIS system[15]. Finalizing the camera lens f/# number is therefore a trade-off between the throughput and image quality and is currently the subject of a study to find the best permutation of filters in the system.

In the MWI optics, the bandpass interference filter which works as a beam splitter is a key optical component. Inappropriate selection of the bandwidth of the filter can cause vignetting across the field of view due to the well-known shift of filter bandpass with incident angle. The influence of the reflective surface in the filter on the image quality in the imaging system is also important and is discussed in detail elsewhere[15]. Here, we present a simulation of the 2D distribution of angle of incident (AOI) on the filter surface to inform the filter bandwidth specification. Figure 4 shows the 2D map of the AOI on the odd channel filter surface. The AOI ranges from 0.5° to 5.5° on all the filters, while the AOI map on even channel is flipped relative to that on an odd channel due to the reflection by the mirrors in the polychromator.

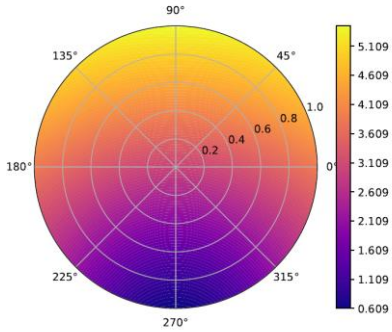

FIG. 4. 2D distribution of angle of incidence (degrees) on the filter surface in odd channels.

III. MECHANICAL DESIGN OF THE MWI SYSTEM

The mechanical parts of the MWI system are designed based on the Zemax optical model. A CAD model of the optical layout generated from Zemax was integrated into the mechanical design to ensure the optics fitted properly into the mechanical parts. The field lens is placed in a commercial kinematic mount in combination with the filter. The camera is mounted to a 5-axis stage in combination with the camera lens. Both mounts have the capability to fine adjust the tilt angle and are attached to a common plate which is installed on a rail guide system, allowing the adjustment of the cavity length by +/-50mm. As discussed in the optical performance section, in-situ focus adjustment is needed if the filter order is changed. Therefore, a calibration arm with a 2-inch diameter integration sphere is implemented and a circular crosshair contact reticle will be install in the intermediate image plane to achieve the in-situ calibration. The calibration arm is placed between lens 3

and lens 4 in the relay optics (see Figure 1), but orthogonal to the original arm, and having the same lens 1-3 optics as the original arm. Access to the calibration arm light path is via a manually-inserted fold mirror (Figure 5).

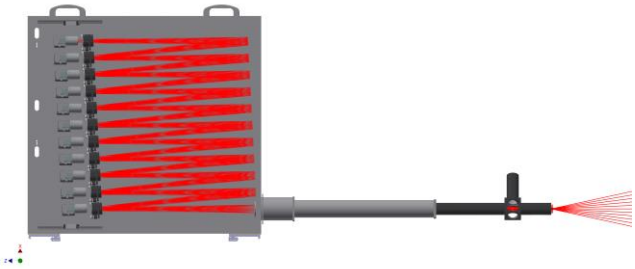

FIG. 5. Mechanical design of MWI system showing the calibration arm. A fold mirror is manually inserted when the calibration arm is in use.

IV. HARDWARE

Most of the optical lenses and mounts used in the MWI system, except for the mirrors and filters, are off-the-shelf products to reduce the time and cost for implementation. As the concave mirrors are located at the position of the intermediate image plane, high specification mirrors with irregularity of ≤¼ lambda, scratch-dig number of 40/20 and a high reflectivity (>99%) dielectric coating in the spectral range 380nm-750nm are used. The bandpass interference filters with high transmission (>90%) in the passband and high reflection (>99.9%) outside the passband are selected to maintain the high throughput and avoid ghost images. Besides the optical components, the synchronization of the cameras and the data acquisition system are of vital importance for the multi-camera diagnostic. For the MWI we choose 11 XIMEA PCIe CMOS cameras with Sony IMX252 sensors. A 12-port switch controls and aggregates all the camera data and transfers the data at up to 8GB/s over a single fiber cable to an acquisition computer. The cameras, data acquisition system and the hardware interface code used in the MWI are the same as those of the MANTIS system which has been tested on the TCV tokamak[15].

V. SYSTEM PERFORMANCE

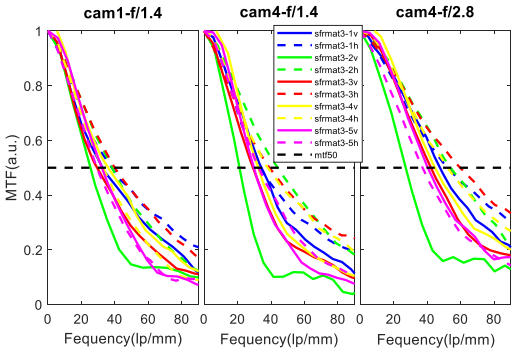

FIG. 6. Measured vertical and horizontal MTFs of Camera 1 and 4 at five different field of views with different apertures in the MWI system.

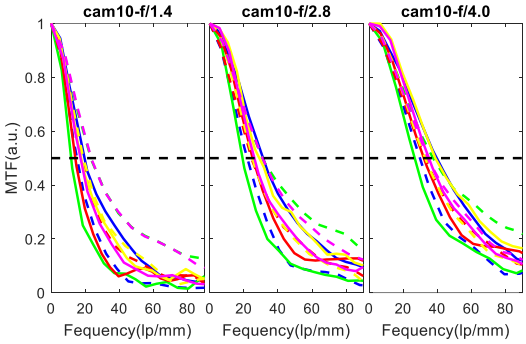

FIG. 7. Measured vertical and horizontal MTFs of Camera 10

For imaging systems, the Modulation Transfer Function (MTF) is a fundamental tool for assessing performance. There are three kinds of targets which may be used to measure the MTF[19]: slanted-edge target, sine-wave target, and grill pattern. Here the MTF of the MWI images is measured using the slanted-edge method, in which multiple slanted-edge targets are placed in the object plane and the horizontal and vertical MTF in five different fields of view (one on axis and rest distributed azimuthally on a ~20° field of view circle) have been measured using the sfrmat3 method[20]. Figure 6 shows the vertical and horizontal MTF of Cameras 1 and 4 with different apertures in the MWI system at the five different field positions. It can be seen in leftmost figure that the average spatial frequency where the MTF reaches a value of 0.5 for Camera 1 with f/1.4 (maximum aperture) is ~35 lp/mm, corresponding to a spatial resolution in the object plane of 330/(2x35) mm=4.7mm, where 330 is the demagnification factor of the optics and the factor 2 corrects for the two lines in a pair. There is slight difference between the vertical and horizontal MTF at each position, which is possibly caused by the astigmatism aberration due to the off-axis system. The middle figure in figure 6 shows that the measured horizontal MTF of Camera 4 at f/1.4 is better than the vertical MTF and even better than the horizontal MTF of Camera 1, but the vertical MTF of Camera 4 is worse than that of Camera 1. This is because the focus for Camera 4 was optimized for the horizontal direction, and not for the vertical direction, which could be corrected by adjusting the focus plane. The average spatial frequency of Camera 4 is similar to that of Camera 1. By stopping down the camera lens to f/2.8 in Camera 4, the average spatial frequency at an MTF value of 0.5 increases due to the improving image quality. The Figure 7 shows the improvement of the overall image quality from stopping down the lens on Camera 10. The average spatial frequency at the MTF value of 0.5 is ~20 lp/mm at f/1.4, corresponding to 8.25mm spatial resolution in the object plane. Stopping down the camera lens to f/4.0 would improve the overall spatial resolution to ~4.5mm. Although the measured image quality of the MWI system is not exactly the same as the that in the simulation in Figure 3, the overall trend of measured image quality with

channel number and camera lens f/# number matches well with the simulation result. The discrepancies between the simulation and measured image quality could be caused by multiple factors, including the non-ideal (non-paraxial) nature of the off-the-shelf camera lens and any residual alignment errors. Figure 8(b) shows the actual divertor view illuminated by a flash lamp. For comparison, the modelled divertor plasma view by CHERAB[21] is shown in figure 8(a).

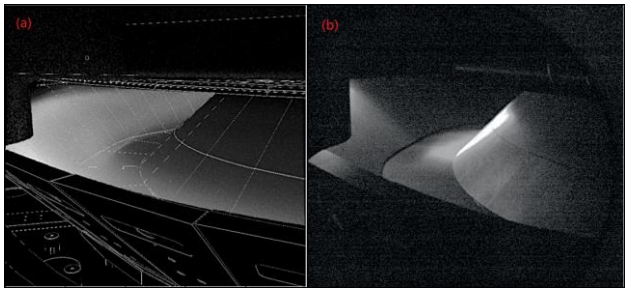

FIG. 8. (a) Modelled divertor plasma view by CHERAB. (b) Actual divertor view illuminated by flash lamp.

Preliminary relative intensity calibration of the MWI system using a 2-inch diameter un-calibrated integrating sphere shows that each channel has a flat response within ±5%. Further absolute calibration of MWI system is ongoing to specify the calibration factors for each pixel in the field of view. Ideally, the full MWI system would be calibrated with an integrating sphere after installation on MAST-U, however, this is not practical for the MWI system as there is no space near the port to put the absolute calibrated integrate sphere close to the system. Therefore, absolute calibration will be made in the laboratory with a calibrated integrate sphere, and in-situ relative intensity calibration with the 2-inch integrating sphere will be employed after installation on MAST-U to regularly check the calibration factor for each pixel.

VI. SUMMARY

An 11-channel Multi-Wavelength Imaging system has been developed for MAST-U to diagnose 2D plasma parameters in the Super-X divertor and explore the influence of magnetic topology on detachment physics. The optical design and mechanical design are described in detail. Optical system performance measurements show less than 5mm FWHM spatial resolution at the plasma can be achieved over the whole field of view. Comparing with previous multi-wavelength imaging systems, the polychromator layout in the MWI reserves the space for integration of other imaging diagnostics, such as Coherence Imaging Spectroscopy to measure 2D impurity flows[16] and electron density maps[17] in the plasma to expand the capabilities of the MWI system.

ACKNOWLEDGMENTS

The authors would like to thank all the CfAI Netpark engineering team for their support during the construction of MWI system. We acknowledge financial support from EPSRC grant EP/N024109/1.This work has been also carried out within the framework of the EUROfusion Consortium and has received funding from the Euratom research and training programme 2014-2018 and 2019-2020 under grant agreement No 633053. The views and opinions expressed herein do not necessarily reflect those of the European Commission.

DATA AVAILABILITY STATEMENT

The data that support the findings of this study are available from the corresponding author upon reasonable request.

REFERENCES

[1]R. A. Pittsa, S. Carpentiera, F. Escourbiaca, T. Hiraia *et al.,* Journal of Nuclear Materials 438, S48-S56 (2013)
[2]A. Loarte, B. Lipschultz, A.S. Kukushkin, G.F. Matthews, P.C. Stangeby *et al.,* Nucl. Fusion, 47, S203-S263 (2007)
[3]B. Lipschultz, F. I. Parra and I. H. Hutchinson, Nucl. Fusion, 56, 056007 (2016)
[4]D. Moulton, J Harrison, B. Lipschultz and D. Coster, Plasma Phys. Control. Fusion, 59, 065011 (2017)
[5]J. R. Harrison *et al.*, Nucl. Fusion, 59, 112011 (2019)
[6]D. Lumma, J. L. Terry, and B. Lipschultz, Phys. Plasmas 4, 2555 (1997).
[7]J. L. Terry, B. Lipschultz, A. Y. Pigarov, S. Krasheninnikov, B. LaBombard *et al.,* Phys. Plasmas 5, 1759 (1998).
[8]J. Karhunena, B. Lomanowskib, V. Solokhaa, S. Aleiferisc, P. Carvalhod *et al.,* Nuclear Materials and Energy, 25, 100831 (2020)
[9]M. Griener, J. M. Burgos, M. Cavedon, G. Birkenmeier, R. Dux *et al.,* Plasma Phys. Controlled Fusion 60, 025008 (2017).
[10]S. Lisgo, P. B¨orner, G. Counsell, J. Dowling, A. Kirk, R. Scannell, M. OMullane, D. Reiter, M. Team *et al*., J. Nucl. Mater. 390-391, 1078 (2009).
[11]O. Schmitz, I. Beigman, L. Vainshtein, B. Schweer, M. Kantor *et al*., Plasma Phys. Controlled Fusion 50, 115004 (2008).
[12]C. Bowman, J. R. Harrison, B. Lipschultz, S. Orchard, K. J. Gibson, M. Carr, K. Verhaegh and O. Myatra, Plasma Phys. Control. Fusion, 62, 045014 (2020)
[13]B. L. Linehan, R. T. Mumgaard, M. Wensing, K. Verhaegh, Y. Andrebe, J. R. Harrison, B. P. Duval, and C. Theiler, Rev. Sci. Instrum. 89, 103503 (2018).
[14]W. A. J. Vijvers, R. T. Mumgaard, Y. Andrebe, I. G. J. Classen, B. P. Duval, and B. Lipschultz, J. Instrum. 12, C12058 (2017).
[15]A. Perek , W. A. J. Vijvers, Y. Andrebe, I. G. J. Classen, B. P. Duval *et al.,* Rev. Sci. Instrum. 90, 123514 (2019).
[16]S. A. Silburn1, J. R. Harrison, J. Howard, K. J. Gibson, H. Meyer, C. A. Michael, and R. M. Sharples, Rev. Sci. Instrum. 85, 11D703 (2014).
[17]J. S. Allcock, New Techniques for Coherence Imaging of Fusion Plasmas, Ph.D. dissertation, Durham University, 2020.
[18]R.T. Mumgaard, *Engineering upgrades to the motional stark effect diagnostic on Alcator C-Mod*, M.Sc. Thesis, Massachusetts Institute of Technology, Cambridge, U.S.A. (2015).
[19]X. Zhang, T. Kashti, D. Kella, T. Frank, D. Shaked, R. Ulichney, M. Fischer, and J. P. Allebacha, Image Quality and System Performance IX, Proc. SPIE 8293, 829307 (2012).
[20]P. D. Burns, D. Williams, Image Quality and System Performance XV, Proc. IS&T Electronic Imaging Symposium, 171 (2018)
[21]C. Giroud, A. Meakins, M. Carr, A. Baciero, and C. Bertrand (2018), "CHERAB spectroscopy modelling framework," Zenodo, version v0.1.0, http://doi.org/10.5281/zenodo.1206142.